OPEN ACCESS
IOP Publishing

Semiconductor Science and Technology

Semicond. Sci. Technol. **36** (2021) 034003 (9pp)

https://doi.org/10.1088/1361-6641/abd924

Improved AlScN/GaN heterostructures grown by metal-organic chemical vapor deposition

Christian Manz[1], Stefano Leone[1], Lutz Kirste[1], Jana Ligl[2], Kathrin Frei[3], Theodor Fuchs[1], Mario Prescher[1], Patrick Waltereit[1], Marcel A Verheijen[4,5], Andreas Graff[6], Michél Simon-Najasek[6], Frank Altmann[6], Michael Fiederle[3] and Oliver Ambacher[1,2]

[1] Fraunhofer Institute for Applied Solid State Physics (IAF), Tullastrasse 72, 79108 Freiburg, Germany
[2] INATECH—Albert-Ludwigs Universität Freiburg, Emmy-Noether-Str. 2, 79108 Freiburg, Germany
[3] Materials Research Center Freiburg, University of Freiburg, Stefan-Meier-Str. 21, 79104 Freiburg, Germany
[4] Eurofins Materials Science Netherlands, High Tech Campus 11, Eindhoven, The Netherlands
[5] Eindhoven University of Technology, PO Box 513, Eindhoven, The Netherlands
[6] Fraunhofer Institute for Microstructure of Materials and Systems (IMWS), Walter-Huelse-Strasse 1, 06120 Halle, Germany

E-mail: stefano.leone@iaf.fraunhofer.de

Received 29 September 2020, revised 18 December 2020
Accepted for publication 6 January 2021
Published 22 January 2021

Abstract

AlScN/GaN epitaxial heterostructures have raised much interest in recent years, because of the high potential of such structures for high-frequency and high-power electronic applications. Compared to conventional AlGaN/GaN heterostructures, the high spontaneous and piezoelectric polarization of AlScN can yield to a five-time increase in sheet carrier density of the two-dimensional electron gas formed at the AlScN/GaN heterointerface. Very promising radio-frequency device performance has been shown on samples deposited by molecular beam epitaxy. Recently, AlScN/GaN heterostructures have been demonstrated, which were processed by the more industrial compatible growth method metal-organic chemical vapor deposition (MOCVD). In this work, SiN_x passivated MOCVD-grown AlScN/GaN heterostructures with improved structural quality have been developed. Analytical transmission electron microscopy, secondary ion mass spectrometry and high-resolution x-ray diffraction analysis indicate the presence of undefined interfaces between the epitaxial layers and an uneven distribution of Al and Sc in the AlScN layer. However, AlScN-based high-electron-mobility transistors (HEMT) have been fabricated and compared with AlN/GaN HEMTs. The device characteristics of the AlScN-based HEMT are promising, showing a transconductance close to 500 mS mm^{-1} and a drain current above 1700 mA mm^{-1}.

Original content from this work may be used under the terms of the Creative Commons Attribution 4.0 licence. Any further distribution of this work must maintain attribution to the author(s) and the title of the work, journal citation and DOI.

 © 2021 The Author(s). Published by IOP Publishing Ltd Printed in the UK

Supplementary material for this article is available online

Keywords: AlScN, ScAlN, aluminum scandium nitride, high electron mobility transistor, MOCVD, atom diffusion

(Some figures may appear in colour only in the online journal)

1. Introduction

The digitalization of society poses many challenges to fulfil the requirements for the transmission of a high volume of data in civil and security applications (from smart devices to radar and satellites) and for efficient conversion of electricity in inverters and converters applied in photovoltaic systems, as well as in electric vehicles, just to name a few examples. High-electron-mobility transistors (HEMT) based on nitride materials (mainly AlGaN alloys) are suited for such high-frequency and high-power electronics applications, thanks to their high switching frequencies, their capacity to withstand high voltages, and to handle high current densities [1]. AlScN can be used as a barrier layer in HEMTs, allowing even higher current densities while reducing switching losses, compared to conventional AlGaN barrier layers. More compact devices with an increased power output can be generated thanks to the physical characteristics of AlScN [2, 3]. The high spontaneous polarization is the main feature of this material, derived from the presence of scandium in the wurtzite-like AlN crystal [4–7]. Epitaxial growth by molecular beam epitaxy (MBE) of AlScN on GaN has already been reported [8–12]. US-based Raytheon and Qorvo have focused on radio-frequency (RF) applications based on AlScN/GaN HEMTs, which achieved simultaneously high current density (>3 A mm^{-1}) and breakdown voltage (>60 V), excellent small-signal RF characteristics at millimeter-wave frequencies [13–15].

A demonstration of its manufacturing can facilitate the acceptance of this new material at an industrial level by the most common highly efficient growth method, already used in the nitride semiconductor industry, i.e. metal-organic chemical vapor deposition (MOCVD). Former attempts to grow scandium-containing nitrides by MOCVD were unsuccessful [16, 17] because of several technological challenges posed by scandium which has different chemistry compared to the standard nitride materials, i.e. gallium and aluminum.

One of the main challenges in the MOCVD growth of Sc-containing nitrides is the absence of a precursor with a vapor pressure high enough to be supplied in industrial MOCVD equipment. As already described in the former attempts of Koleske *et al* [16], tris-cyclopentadienyl-scandium (Cp_3Sc) is the best choice among the very few commercially available Sc-precursors. We have recently demonstrated that the MOCVD growth of AlScN is possible by a proper rearrangement of the gas mixing system in commercial MOCVD equipment [18]. Due to its low vapor pressure, the source material and the gas lines up to the gas injection system were heated to a temperature of 150 °C. Through a proper set-up, which also included a mass flow controller to regulate the amount of hydrogen flowing through the bubbler and a pressure gauge, we could control and supply a molar flow of Cp_3Sc in the reaction chamber succeeding in depositing epitaxial AlScN layers at a rate close to 0.1 μm h^{-1} and with an Sc-concentration up to 30%.

Recently, we have also reported on the effect of the primary growth parameters on the quality of epitaxial AlScN/GaN heterostructures [19]. The effect of temperature, V/III ratio, pressure and metal supply were investigated for the growth of 50–100 nm thick epitaxial layers, with a final focus on thin AlScN/GaN heterostructures in the successful attempt to have suitable material for the fabrication of HEMTs. Similar to other nitrides, we found a positive impact by the use of higher growth temperature, pressure and V/III ratio, especially in terms of impurity reduction and electrical characteristics of the AlScN/GaN heterostructures. At the same time, some challenges arose. For example, the GaN cap used to protect and passivate the AlScN barrier layer had low morphological quality, consisting of three-dimensional islands for growth temperatures below 1200 °C. Such a cap layer could not prevent the exposure of the AlScN barrier layer to the atmosphere, which caused oxidation of the same. Besides, transmission electron microscopy (TEM) analysis not only confirmed the poorly coalesced GaN cap layer but also indicated the presence of several structural defects at the interface between the GaN channel and the AlScN barrier layer. Finally, yet importantly, the crystal quality of the AlScN layer could not be considered sufficient to eventually deliver a high-quality HEMT. However, the electrical characteristics were quite comparable with those achieved by MBE-grown AlScN/GaN heterostructures.

The difficulties mentioned above have not been addressed so far. However, they are fundamental challenges to be overcome and to bring AlScN to its full potential even when grown by MOCVD, which is the technique with the highest productivity adopted in the nitride semiconductor industry.

In this work, we developed a MOCVD process for the deposition of a coalesced passivation layer based on *in-situ* grown silicon nitride (SiN_x) for AlScN/GaN heterostructures, considering that such a passivation layer is already successfully employed on standard nitrides HEMTs for high-power and high-frequency applications [20–22]. Besides, SiN_x passivated AlScN/GaN heterostructures have never been investigated so far, to the best of our knowledge. We also focused on tuning the growth mode (continuous or pulsed mode) of thin (5–10 nm) AlScN barrier layers. We compared the morphology of cap layers and the structural quality of the barrier layer. TEM analysis corroborated by energy-dispersive x-ray spectroscopy (EDX) is used to confirm the better quality of the SiN_x cap, but also to understand the structural quality and the chemical composition of the AlScN barrier layer deposited at different temperatures and growth modes. A comprehensive

TEM characterization was conducted to monitor the presence of structural defects formerly reported [19]. Special attention was also devoted to the distribution of Sc, Al and Ga atoms in the key layers with EDX measurements, to understand if diffusion or segregation problems exist as seen in the former analysis. Indeed, it is well known that Al and Ga [23], as well as other elements such as Mg [24] and Fe [25], tend to diffuse strongly between the nitride layers due to the high growth temperatures commonly adopted in the MOCVD process [26]. Therefore, special attention was paid to understand if Sc also shows a similar diffusion behavior. High-resolution x-ray diffraction (HRXRD) and secondary ion mass spectrometry (SIMS) were employed to analyze the crystal and interface quality, as well as the composition of the presented heterostructures. Finally, transistors have been fabricated on SiN_x-passivated thin AlScN/GaN heterostructures to get a first understanding on the quality of such layers and compared to SiN_x-passivated AlN/GaN heterostructure deposited in the same MOCVD reactor.

2. Experimental part

The epitaxial growth of all presented structures was carried out in a close-coupled showerhead MOCVD reactor, as described in our earlier works [18, 19]. Ammonia (NH_3) was used to provide the group-V element, while trimethylgallium and trimethylaluminum were used as group-III precursors, and silane (SiH_4) was the precursor for the SiN_x cap layer. For the supply of scandium, tris-cyclopentadienyl-scandium (Cp_3Sc) was used. Hydrogen served as the carrier gas in all experiments, which were conducted in a low-pressure regime (40–100 mbar) and a growth temperature between 1000 °C and 1200 °C.

In this work, epitaxial AlScN/GaN heterostructures, either with *in-situ* grown GaN or SiN_x cap layer, are compared. The growth parameters for the deposition of the AlScN barrier layer were varied in terms of metal supply (pulsed or continuous) and a growth temperature (1000 °C, 1100 °C and 1200 °C); otherwise, the growth parameters as well as the epitaxial layer stack were the same as those described in our previous work [19]. The barrier layers are conventionally grown with continuous metal supply, which means that both TMAl and Cp_3Sc, are supplied simultaneously for the whole barrier growth duration. For pulsed metal supply, the two precursors were injected separately into the growth chamber, with different pulse durations: the Cp_3Sc supply was open for 5 s while TMAl supply was off, then the Cp_3Sc supply was off for 2 s while TMAl supply was open. The cap layer was either a 2 nm GaN or a 5–10 nm SiN_x layer deposited in continuous growth mode at the same temperature and pressure as the barrier layer. Typically, 100 mm on-axis sapphire substrates were used, but occasionally also semi-insulating 4H-SiC substrates were employed, especially for those samples that were also used to fabricate transistors. For the sake of comparison, also a heterostructure with an AlN barrier layer was deposited (sample 7) at similar growth conditions of another sample with AlScN barrier (sample 6). The typical epitaxial layers sequence is reported in the supplementary information (S1) (available online at stacks.iop.org/SST/36/034003/mmedia).

A summary of the epitaxial heterostructures discussed in this work is reported in table 1.

The surface morphology of the heterostructures was analyzed by atomic force microscopy (AFM) in tapping mode. The morphology, crystallographic structure and qualitative elemental composition of the layers were investigated by high-resolution TEM imaging and STEM/EDX analysis at two different sites: Fraunhofer IMWS and Eurofins Material Science Netherlands B.V. (EAG). Bright-field TEM and high-angle annular dark-field (HAADF) detectors were used to inspect the structural quality and defect formation of the layers. Electron transparent samples for the TEM analysis were prepared using the focused ion beam (FIB) lift-out method [27]. Because of the high effort of TEM analysis, only a few carefully selected samples were analyzed. In addition to the TEM investigations, HRXRD and x-ray reflectometry (XRR) measurements were performed to determine layer thickness, phase purity and material quality. The composition of the layers was analyzed by SIMS on some selected sample, where Cs^+ ions with 1 keV or 5 keV energy were used as the primary ion beam to identify secondary ions or molecules containing Sc, Al, Ga, Si and N, but also impurities such as C, and O in the epitaxial layers. Further, sheet resistance, mobility and sheet carrier density were measured by either eddy-current sheet resistance measurements or Hall measurements in Van der Pauw geometry using In–Ga or Ti–Al contacts.

Device processing on sample 6 (AlScN-barrier layer) and 7 ($Al_{0.6}Ga_{0.4}N$-barrier layer) was carried out using both, electron-beam and stepper lithography. It involves isolation by implantation, alloyed Ti/Al-based ohmic contacts optimized for low contact resistance (below 0.25 Ω mm) and smooth edges for improved marker recognition. The gate is defined by electron beam lithography. The gate head is designed to achieve low parasitic capacitances, which is essential for high-speed operation. SiN_x passivation optimized for low current dispersion and thermal stability is deposited. Furthermore, fabrication of integrated circuits comprises the processing of NiCr thin-film resistors, MIM (metal–insulator–metal) capacitors, interconnect metals, electroplated Au airbridges, and inductors.

3. Results and discussion

This paragraph is divided into four sections, showing the following layer properties determined by different analysis methods: surface morphology by AFM, morphology, crystallographic structure and elemental composition by TEM and STEM/EDX, crystal structure and interface sharpness by HRXRD and XRR, and finally electrical properties of HEMTs.

3.1. Morphological analysis of the cap layer

In our previous work, we showed that the GaN cap grown on top of the AlScN layer at temperatures below 1200 °C generates 3D islands, resulting in a not-coalesced layer and,

Table 1. Summary of growth parameters, layer thickness results obtained by HRXRD and XRR, assuming a homogeneous AlScN layer. The HRXRD measurements could not resolve the AlN interlayer thickness for samples where it was inserted (samples 1–4), so the nominally adjusted values are listed. The Sc concentration was determined by SIMS for all investigated samples, except for those marked with **, whose Sc-concentration was assumed to be the same as that of samples where the AlScN was grown exactly with the same growth parameters. *Sample 7 is a heterostructure with an intentionally pure AlN barrier layer, without Sc. Due to Al- and Ga-atoms diffusion between the layers grown at high-temperature, we estimate that instead of AlN a gradient layer with a mean composition of $Al_{0.6}Ga_{0.4}N$ was formed.

Cap layer	GaN	SiN_x	GaN	SiN_x	SiN_x	SiN_x	SiN_x
Sample ID	1	2	3	4	5	6	7
Growth temperature (°C)	1000	1000	1200	1200	1100	1100	1100
Growth mode	Pulsed	Pulsed	Contin.	Contin.	Contin.	Contin.	Contin.
Cap layer thickness (nm)	3	3.1	1	9.3	4.4	3.4	3
AlScN barrier layer thickness (nm)	6.5	16.9	9	10.3	9.9	9.5	5.6*
Sc concentration (%)	13.7	9.8	17	17**	5	14**	—
AlN interlayer thickness (nm)	2	2	2	2	—	—	—
Substrate	Al_2O_3	Al_2O_3	Al_2O_3	Al_2O_3	Al_2O_3	4H-SiC	4H-SiC

consequently, insufficient passivation and protection of the barrier layer from the atmosphere, mainly from oxidation. It was deduced by AFM measurements and further evidenced by TEM analysis [19], and it was also observed in this work. The AFM picture of a GaN cap layer grown at 1000 °C (sample 1) is shown in figure 1(a). The root means square (RMS) roughness of this GaN/AlScN/GaN heterostructure is 1.5 nm for an AFM scan area of 2 × 2 μm^2, which is comparable to RMS values in our earlier work. In figure 1(b), the AFM picture of the 2 × 2 μm^2 scan of sample 2 with SiN_x cap is shown representatively for the samples of the SiN_x cap series. In comparison to sample 1, the RMS roughness is remarkably lower with only 0.2 nm. Furthermore, a completely closed SiN_x cap layer can be observed from the AFM picture, whereas a smooth layer free of pits or deep valleys is visible, indicating successful passivation of the underlying AlScN barrier.

All the other samples (3–7) grown at higher temperature show a closed cap layer, as it was deduced by AFM measurements for both, the GaN and the SiN_x cap layer, respectively. The measured AFM RMS for samples grown at 1200 °C (samples 3 and 4) was 0.1 nm. We can conclude that the SiN_x cap layer leads to a coalesced and uniform passivation layer regardless of the growth temperature, which is not the case for the GaN cap layer.

3.2. Layer structure and elemental composition analyzed by TEM and STEM/EDX

TEM measurements were performed on samples with a GaN cap (sample 1) and SiN_x cap layer (sample 4). Figure 2 shows high-resolution (HR) TEM images (<01-10> zone axis) of these two samples. The sample with the GaN cap layer (sample 1) has a not-coalesced cap layer consisting of GaN islands. The SiN_x cap layer (sample 4), on the other hand, has a closed surface over the whole measurement range, which is consistent with the above-presented results from AFM.

In the depicted AlScN barrier layers, structural defects can be observed on the sample grown in pulsed mode (sample 1, figures 2(a) and (b)), recognizable by the contrast variations. No distinct structural defects could be discerned at atomic resolution in the HRTEM images, acquired using an image corrected TEM. It is plausible that these defects are not intrinsic to the AlScN growth, but are the result of post-growth oxidation that has occurred through the uncoalesced GaN cap. Similar structural defects have not been observed in the sample deposited in continuous mode (sample 4, figures 2(c) and (d)). An extended TEM study comprising weak beam imaging and HRTEM and probe-corrected STEM imaging of the same sample under <01-10> and <2-1-10> zone axes did not show any structural defects, apart from the low density of threading dislocations originating from the substrate/buffer layer interface. From the images acquired in HAADF-STEM mode, which provides atomic number contrast (S2), it can be noticed that there is not an atomically sharp interface between the GaN buffer and the AlScN barrier layer, besides the fact that the intended AlN interlayer between the GaN channel and AlScN barrier cannot be seen as well.

Bright field HRTEM images of samples 4 and 6 along the <2-1-10> zone axis were taken as well (available in the supplementary information). Indeed, the atomic spacings are slightly larger in the <2-1-10> zone axis images and, more importantly, the <2-1-10> zone axis allows for discrimination between hexagonal and cubic stacking. In both samples, no cubic stacking could be seen.

In addition to the structural TEM investigation, the elemental composition across the layer structure was determined by STEM/EDX mappings, as shown in figure 3 for samples 1(a) and 4(b). The GaN buffer layer, the AlScN barrier layer, and the GaN or SiN_x cap layer can be seen in the growth direction from bottom to top. The results indicate a very well defined and closed SiN_x cap layer (sample 4), resulting in successful passivation of the AlScN barrier-free of oxygen contamination. The barrier topped with the GaN cap (sample 1), on the other hand, has undergone severe oxidation mainly at the locations not covered by the GaN cap, as seen by the presence of oxygen in the AlScN layer.

Furthermore, it can be seen that there is a non-uniform lateral distribution of Sc and Al in the barrier layer of sample 1 (grown in pulsed mode at low temperature), whereas a graded

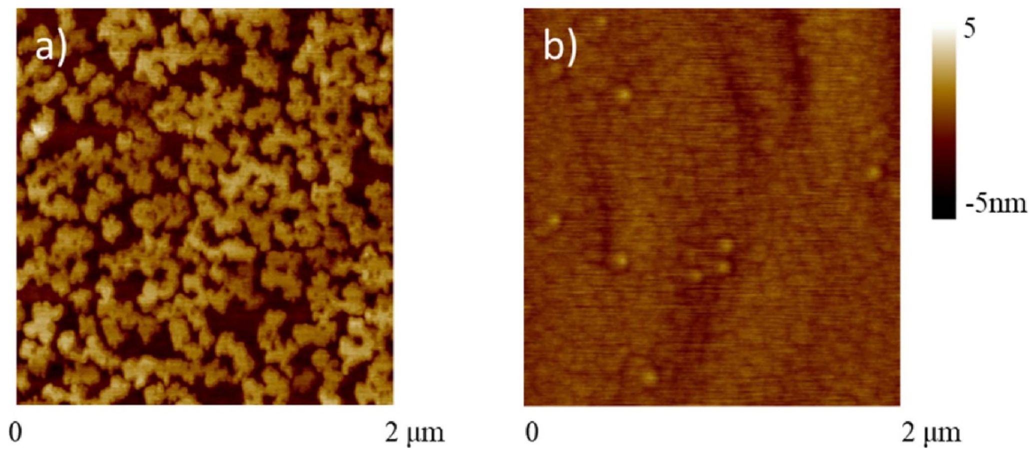

Figure 1. 2×2 μm^2 AFM scan of: (a) sample 1 with GaN cap layer, with RMS = 1.5 nm; (b) sample 2 with SiN_x cap layer, with RMS = 0.2 nm.

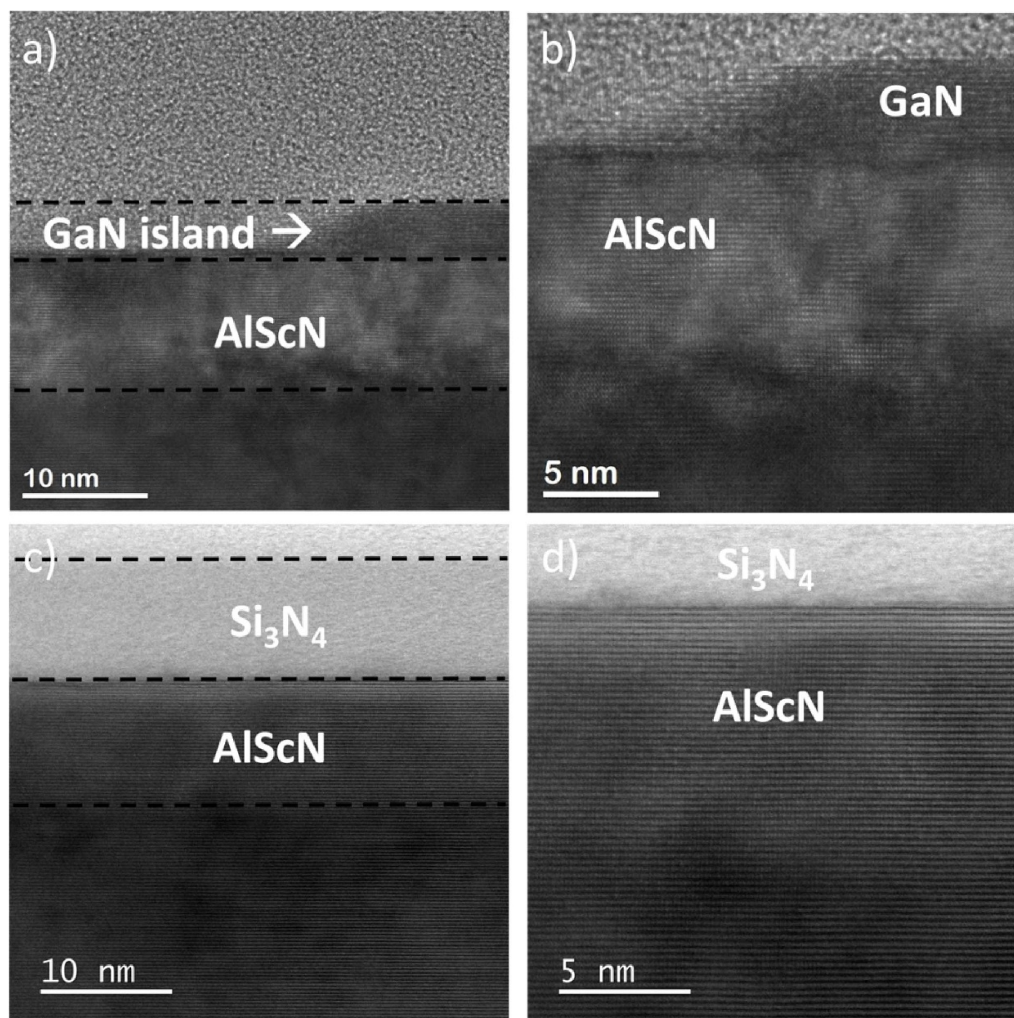

Figure 2. Bright field HRTEM images (<01-10> zone axis) at different magnifications of a cross section of: (a) and (b) GaN capped sample (sample 1), where the GaN cap consists of GaN islands. The AlScN layer seems to have several structural defects. (c), (d) SiN_x capped sample (sample 4), where the successful growth of a completely closed SiN_x-cap layer is visible (as shown by AFM analysis), and structural defects are not visible in the AlScN layer. The dashed line markers are used only as a guide for the eye.

vertical distribution of Sc and Al in the barrier layer was detected in sample 4 (grown in continuous mode at high temperature). In the latter case, Sc is detectable in the last 5 nm close to the cap layer, whereas a significant amount of Al diffused into the GaN buffer layer. Apparently, Al diffused deeply into the GaN buffer layer, and Sc was located mainly in the outermost

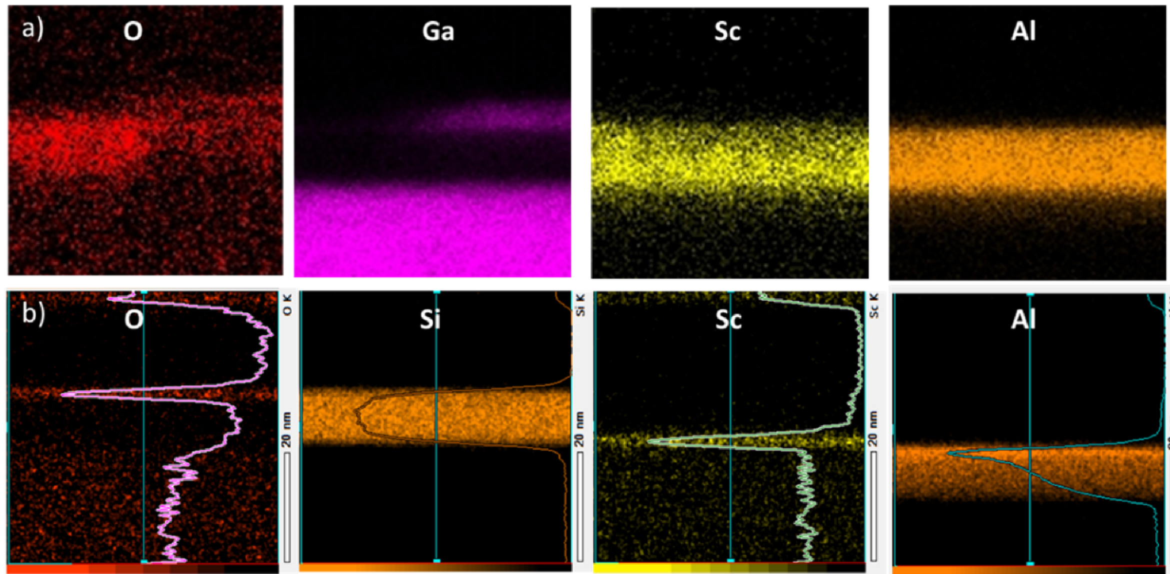

Figure 3. Elemental distribution of STEM-EDX mappings for: (a) the GaN/AlScN/GaN heterostructure, with the AlScN layer deposited in pulsed growth mode (sample 1); (b) the SiN_x/AlScN/GaN heterostructure, with the AlScN layer deposited in continuous growth mode (sample 4). The traces superimposed over the elemental mappings in figure (b) are the raw EDX counts profiles along the vertical direction, summed over the entire width of the mapping.

part of the barrier layer. Such a substantial diffusion of Al into the GaN buffer layer is a well-known effect also seen in Al(Ga)N barrier layers [26]. In spite of the small thickness of the AlScN layer in sample 4, we can assess the absence of a non-uniform lateral distribution of Al and Sc, which was the case of sample 1.

The clear evidence of a non-uniform vertical distribution of Al and Sc across the heterostructure (sample 4), points out the need of further MOCVD process optimization, mainly to prevent the well-known problem of Al-diffusion during high-temperature processes. Nevertheless, as will be shown later, this class of samples with AlScN grown in continuous mode shows good electrical performance. Such experimental evidence allows us to speculate that the lateral distribution of Sc and Al in the AlScN layers grown in continuous mode (such as in sample 4, or sample 6 shown in the supplementary information) is negligible because it does not affect the electrical characteristics of this heterostructure.

3.3. Structural properties and interface sharpness analyzed by HRXRD and XRR

Additional structural information was obtained by HRXRD and XRR measurements performed on all the samples listed in table 1.

Figure 4(a) shows the Θ/2Θ-scans of the 0002 reflection range for the investigated samples. It has to be mentioned that sample 1 was replaced with another sample grown with identical growth parameters except for a higher V/III ratio, due to the unavailability of sample 1 for HRXRD analysis.

In addition to the strong and sharp reflection of the GaN buffer layers, weaker and broader reflections of the thin barrier layers and the AlN interlayers can be seen. Additionally, thickness fringes of the thin AlScN barrier layers, the AlN interlayers and the GaN cap, if a GaN cap has been grown, are observed in the diffractograms. The thickness fringes have a blurred appearance with low dynamic. However, sample 2, deposited at 1000 °C and with a SiN_x-cap, shows the most pronounced fringes. No thickness fringes are visible in the HRXRD measurements for the samples with a SiN_x-cap layer because the SiN_x-cap is amorphous. Since the diffraction Θ/2Θ-pattern of 0002 reflection ranges show an indefiniteness of the layers´ structure in terms of interface quality and homogeneity, additional Θ/2Θ-scans of 0004 (figure 4(b)) and 0006 (not shown) were performed to understand the structural characteristics of the samples better.

In the Θ/2Θ 0004 scan ranges, very low intensities are observed for the AlScN layer reflections. Besides, the reflection appear significantly broadened, which cannot only be attributed to the layers´ low thicknesses but also indicates inhomogeneities regarding the Sc distributions. This interpretation is also supported by the asymmetrical shapes of the barrier reflections. Thickness fringes, except for samples 1 and 2, are not observed in the 0004 reflection pattern indicating a suboptimal surface or interface quality. By taking into account the results of the TEM imaging, STEM/EDX and SIMS analysis (not shown here) into the interpretation of these HRXRD Θ/2Θ profiles, it is clear that the layer stacks grown on the GaN buffer layers, consisting of AlN interlayer, AlScN barrier and cap layer, do not have sharp boundaries but a significant mixing of the different material layers. Therefore, the observed reflection positions and thickness fringes of the AlN interlayer, AlScN barrier and cap layer cannot be differentiated and precise structural analysis of the single layers of the layer stacks is not possible using HRXRD. The higher quality of the thickness fringes observed for sample 1 is due to a thicker AlN (or AlGaN) interlayer when taking into account

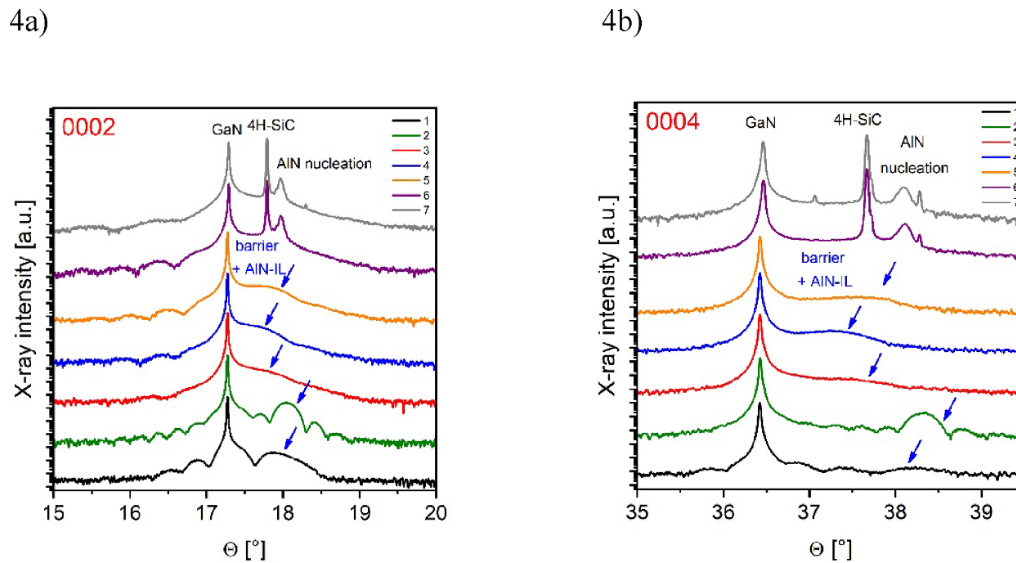

Figure 4. Θ/2Θ-scan of the 0002 reflection range (a) and of the 0004 reflection range (b) for the six investigated AlScN/GaN samples and the AlN/reference (sample 7) sample as described in table 1.

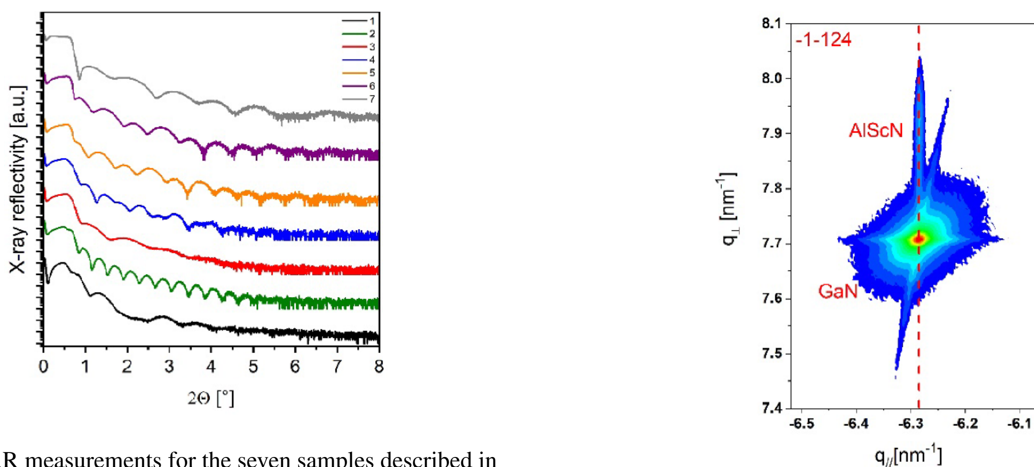

Figure 5. XRR measurements for the seven samples described in table 1.

Figure 6. HRXRD reciprocal space mapping of the $\bar{1}\bar{1}24$ reflection range of sample 5.

the SIMS results and does not represent the quality of the nominal AlScN barrier.

The reflection range of the barrier regions is overlaid by the 4H-SiC substrate reflection in the HRXRD pattern of the samples 6 and 7 deposited on the 4H-SiC substrate, one with a nominal AlScN barrier and the other with a nominal pure AlN barrier, respectively. The reflection of the AlN nucleation layer and the exact position of the AlScN reflection is therefore not visible (figures 4(a) and (b)). However, material carryover and low interface quality can also be assumed for these two samples due to the low thickness fringe quality.

In order to improve the data situation for the determination of the thicknesses of the barrier layers, the amorphous SiN_x- or crystalline GaN-cap layers and AlN interlayers, and to determine the surface and interface quality for the different HEMT structures, XRR measurements were performed (figure 5).

The XRR profiles of the sample series show pronounced thickness fringes for the samples with SiN_x-cap, but for sample 1 and sample 3 with the GaN-cap, the dynamic of the fringes is strongly damped. This can be explained by the island-like 3D growth of the GaN-cap layers. When an amorphous SiN_x-cap layer is used, the layers are closed, and the XRR profiles show fringes with better quality. In general, for the whole series of samples, it has to be stated that for the simulations of the XRR profiles (not shown) it was impossible to generate models of heterostructures with sharp interfaces, for the reasons as described for the analysis of the HRXRD pattern.

Finally, HRXRD reciprocal space mappings of the $\bar{1}\bar{1}24$ reflection range were performed to determine the strain state of the AlN interlayers, AlScN barriers and if used the GaN cap layers in relation to the GaN buffer layers. Figure 6 shows as an example the $\bar{1}\bar{1}24$ reciprocal space mappings of sample 5.

The reciprocal space mappings of all samples indicate the growth of fully strained layer stack on top of the GaN buffers,

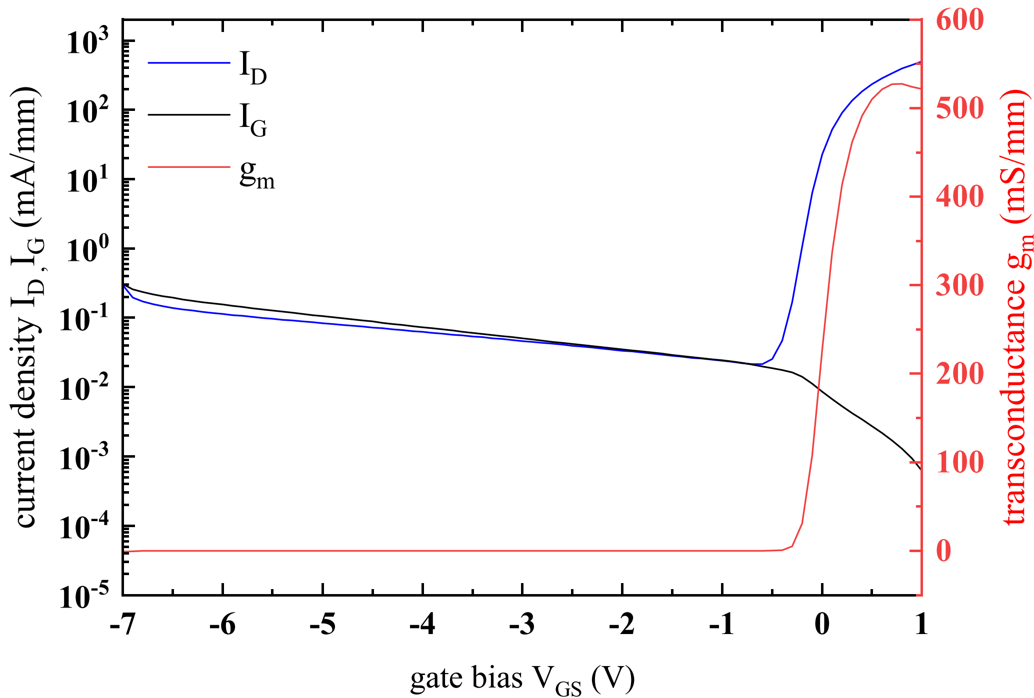

Figure 7. Transfer characteristic of a device obtained on sample 6 (AlScN barrier layer) with a gate length L_g of 0.25 μm and a drain bias of 7 V showing a maximum transconductance g_m of 530 mS mm^{-1} and a drain current of 1.72 A mm^{-1}.

illustrated by the dashed line (red) in figure 6. Regarding thickness and estimated Sc concentration of the barrier layers, it is noteworthy that the presence of the strained layer stack region in sample 5 additionally confirms the occurrence of graduated interfaces and material mixing. According to theoretical calculations by Zhang *et al* [28], the critical thickness of $Al_{0.95}Sc_{0.05}N$ is only 6 nm; hence relaxation effects should be visible for strained epitaxially grown layers of consistent composition and high phase purity.

We can conclude that the HRXRD and XRR results confirm the observations by AFM, TEM and STEM/EDX, which are: the absence of sharp interfaces and surfaces, material mixing as well as an inhomogeneous Sc distribution.

Table 2. Comparison of the electron transport properties of the MOCVD-grown AlScN and AlN barrier HEMTs.

	Sample 6 (AlScN barrier)	Sample 7 (AlN barrier)
Sheet resistance (Ω sq^{-1})	323	325
Mobility (cm^2 V s^{-1})	729	726
Carrier conc. (10^{13} cm^{-2})	2.6	2.6
Transconductance (mS mm^{-1})	530	660
Drain current (mA mm^{-1})	1720	1700

3.4. Processed devices structures

In order to have a final evaluation of the material properties of the discussed AlScN heterostructures, HEMTs were fabricated as discussed in the experimental section, and a comparison of their electrical properties is presented in the following. In table 2 the characteristics and electron transport properties of such SiN_x/AlScN/GaN (sample 6) and SiN_x/AlN/GaN (sample 7) HEMTs are shown. It can be noted that, despite the different barrier materials, the properties of the 2DEG are comparable, which indicates that successful device fabrication of AlScN barrier HEMTs grown by MOCVD could be achieved. Furthermore, the similarity of carrier concentration and electron mobility, which are below the theoretically expected values [8], are a result of heavy interdiffusion of the metal atoms Al, Ga, and Sc in the buffer and barrier, as evidenced by STEM/EDX and HRXRD analysis. Therefore, it can be assumed that the barrier of samples 6 and 7 consists of a high Al-content AlGaScN and AlGaN layer, respectively. It is also worth mentioning that the measured mobilities are lower than the typically measured values reported in the literature for the AlN barrier layer [29]. The primary source for the lower mobility in both samples are most likely the poor interface quality and the atoms interdiffusion, causing alloy scattering, which is known to affect the mobility of HEMT heterostructures [30].

In figure 7, the gate and drain leakage currents are shown in a semilogarithmic plot of sample 6 (AlScN barrier layer). The maximum transconductance amounts to 530 mS mm^{-1} and a drain current up to 1720 mA mm^{-1} was achieved. Generally, the transfer characteristics of these preliminary AlScN transistors fabricated on a 100 mm 4H-SiC S.I. substrate are very promising results for future high power and high-frequency applications, already superior to standard AlGaN HEMT for RF applications fabricated in-house [31].

4. Conclusions

In this work, we have focused on improving the quality of AlScN barrier layers grown by MOCVD and the morphology of the cap layer needed for HEMT heterostructures. AFM and (HR)TEM analysis have shown that an *in situ* grown SiN_x passivation layer is an ideal cap layer compared to GaN, because it results in a coalesced layer regardless of the growth temperature, avoiding oxidation of the AlScN layer. Besides, the growth in continuous mode of an optimized AlScN barrier layer seems to be free of structural defects. However, severe diffusion of atoms between the barrier and channel layers occur. Lateral non-uniform distribution of Sc and Al can be noted for the AlScN layer grown in pulsed mode, while a strong Al diffusion from the barrier into the GaN layer occurs in all cases. This diffusion effect is also clearly visible in the HRXRD and XRR analysis, where the absence of sharp interfaces and inhomogeneities in the alloy composition makes the assessment of layer thicknesses difficult. Nevertheless, HEMTs were fabricated on SiN_x/AlScN/GaN heterostructures deposited on 4H-SiC S.I. and showed very promising performances with high transconductance and drain current.

The results achieved in this work show that MOCVD-grown AlScN-based HEMT have good electrical performance. However, further optimizations are required to improve the crystal quality, achieve sharp interfaces for the layer stacks, and obtain uniform alloy composition between the layers, in order to achieve the expected performance of Sc-based HEMT.

Acknowledgments

The authors would like to acknowledge Dr K Köhler for useful discussions and relevant contributions in the preparation of the manuscript. The authors would also like to thank all the colleagues at IAF who have helped in the material preparation, characterization, wafer processing, and administration of the internal research project, especially H Menner, J Richter and J Wiegert.

ORCID iD

Christian Manz https://orcid.org/0000-0002-1706-1905

References

[1] Quay R, Bruckner P, Tessmann A, Ture E, Schwantuschke D, Dammann M and Waltereit P 2017 *Integrated Nonlinear Microwave and Millimetre-wave Circuits Workshop (INMMiC 2017)* (*20 –21 April 2017 Graz, Austria*) (Piscataway, NJ: IEEE) p 1–3
[2] Moram M A and Zhang S 2014 *J. Mater. Chem.* A **2** 6042
[3] Höglund C, Birch J, Alling B, Bareño J, Czigány Z, Persson P O Å, Wingqvist G, Zukauskaite A and Hultman L 2010 *J. Appl. Phys.* **107** 123515
[4] Akiyama M, Kamohara T, Kano K, Teshigahara A, Takeuchi Y and Kawahara N 2009 *Adv. Mater.* **21** 593
[5] Tasnadi F, Alling B, Höglund C, Wingqvist G, Birch J, Hultman L and Abrikosov I A 2010 *Phys. Rev. Lett.* **104** 137601
[6] Tholander C, Abrikosov I, Hultman L and Tasnádi F 2013 *Phys. Rev.* B **87** 094107
[7] Caro M A, Zhang S, Riekkinen T, Ylilammi M, Moram M A, Lopez-Acevedo O, Molarius J and Laurila T 2015 *J. Phys.: Condens. Matter.* **27** 245901
[8] Hardy M T, Downey B P, Nepal N, Storm D F, Katzer D S and Meyer D J 2017 *ECS Trans.* **80** 161
[9] Hardy M T, Downey B P, Nepal N, Storm D F, Katzer D S and Meyer D J 2017 *Appl. Phys. Lett.* **110** 162104
[10] Hardy M T, Jin E N, Nepal N, Katzer D S, Downey B P, Gokhale V J, Storm D F and Meyer D J 2020 *Appl. Phys. Express* **13** 65509
[11] Frei K, Trejo-Hernández R, Schütt S, Kirste L, Prescher M, Aidam R, Müller S, Waltereit P, Ambacher O and Fiederle M 2019 *Japan. J. Appl. Phys.* **58** SC1045
[12] Casamento J, Chang C S, Shao Y-T, Wright J, Muller D A, Xing H and Jena D 2020 *Appl. Phys. Lett.* **117** 112101
[13] Kazior T E, Chumbes E M, Schultz B, Logan J, Meyer D J and Hardy M T 2019 *IEEE MTT-S International Microwave Symposium (IMS 2019)* (*2–7 June 2019 Boston, MA*) (Piscataway, NJ: IEEE)1136–9
[14] Green A J *et al* 2019 *IEEE Electron Device Lett.* **40** 1056
[15] Green A J *et al* 2020 *IEEE Electron Device Lett.* **41** 1181
[16] Koleske D, Knapp J A, Lee S R, Crawford M H, Creighton J R, Cross K C and Thaler G 2009 Issues associated with the metal-organic chemical vapor deposition of ScGaN and YGaN alloys (https://doi.org/10.2172/961650)
[17] Saidi C, Chaaben N, Bchetnia A, Fouzri A, Sakly N and El Jani B 2013 *Superlattices Microstruct.* **60** 120
[18] Leone S *et al* 2019 *Phys. Status Solidi RRL* **14** 1900535
[19] Ligl J, Leone S, Manz C, Kirste L, Doering P, Fuchs T, Prescher M and Ambacher O 2020 *J. Appl. Phys.* **127** 195704
[20] Derluyn J, Boeykens S, Cheng K, Vandersmissen R, Das J, Ruythooren W, Degroote S, Leys M R, Germain M and Borghs G 2005 *J. Appl. Phys.* **98** 54501
[21] Germain M, Cheng K, Derluyn J, Degroote S, Das J, Lorenz A, Marcon D, van Hove M, Leys M and Borghs G 2008 *Phys. Status Solidi* C **5** 2010
[22] Dogmus E, Kabouche R, Linge A, Okada E, Zegaoui M and Medjdoub F 2017 *Phys. Status Solidi* a **214** 1600797
[23] Leone S, Brueckner P, Kirste L, Doering P, Fuchs T, Mueller S, Prescher M, Quay R and Ambacher O 2020 *Phys. Status Solidi* b **257** 1900436
[24] Köhler K, Gutt R, Wiegert J and Kirste L 2013 *J. Appl. Phys.* **113** 073514
[25] Leone S, Benkhelifa F, Kirste L, Manz C, Mueller S, Quay R and Stadelmann T 2018 *Phys. Status Solidi* b **255** 1700377
[26] Godejohann B-J *et al* 2017 *Phys. Status Solidi* B **254** 1600715
[27] Simon-Najasek M, Huebner S, Altmann F and Graff A 2014 *Microelectron. Reliab.* **54** 1785–9
[28] Zhang S, Holec D, Humphreys C J and Moram M A 2013 *J. Appl. Phys.* **114** 133510
[29] Meneghesso G, Meneghini M, Medjdoub F, Tagro Y, Grimbert B, Ducatteau D, Rolland N, Silvestri R and Zanoni E 2013 *IEEE Trans. Device Mater. Reliab.* **13** 480
[30] Jena D, Smorchkova I, Gossard A C and Mishra U K 2001 *Phys. Status Solidi* B **228** 617–9
[31] Leone S, Godejohann B J, Brueckner P, Kirste L, Manz C, Swoboda M, Beyer C, Richter J and Quay R. 2018 *Int. Conf. on Compound Semiconductor Manufacturing Technology (CS Mantech 2018)* (*7–10 May 2018 Austin, TX*)